# Excitatory/inhibitory neuronal metabolic balance in mouse hippocampus upon infusion of [U-$^{13}$C$_6$]glucose

Antoine Cherix[1] ⓘ, Guillaume Donati[1], Blanca Lizarbe[1,2] ⓘ,
Bernard Lanz[1,3], Carole Poitry-Yamate[1], Hongxia Lei[4] ⓘ and
Rolf Gruetter[1]

## Abstract

Hippocampus plays a critical role in linking brain energetics and behavior typically associated to stress exposure. In this study, we aimed to simultaneously assess excitatory and inhibitory neuronal metabolism in mouse hippocampus in vivo by applying $^{18}$FDG-PET and indirect $^{13}$C magnetic resonance spectroscopy ($^1$H-[$^{13}$C]-MRS) at 14.1 T upon infusion of uniformly $^{13}$C-labeled glucose ([U-$^{13}$C$_6$]Glc). Improving the spectral fitting by taking into account variable decoupling efficiencies of [U-$^{13}$C$_6$]Glc and refining the compartmentalized model by including two $\gamma$-aminobutyric acid (GABA) pools permit us to evaluate the relative contributions of glutamatergic and GABAergic metabolism to total hippocampal neuroenergetics. We report that GABAergic activity accounts for $\sim$13% of total neurotransmission ($V_{NT}$) and $\sim$27% of total neuronal TCA cycle ($V_{TCA}$) in mouse hippocampus suggesting a higher $V_{TCA}/V_{NT}$ ratio for inhibitory neurons compared to excitatory neurons. Finally, our results provide new strategies and tools for bringing forward the developments and applications of $^{13}$C-MRS in specific brain regions of small animals.

## Keywords

$^1$H-[$^{13}$C]-MRS, neuronal metabolism, metabolic modeling, TCA cycle, mouse hippocampus

Received 31 August 2019; Revised 30 January 2020; Accepted 7 February 2020

## Introduction

The hippocampus plays a critical role in linking brain energetics and neurotransmission to behavior in response to stress exposure.[1,2] The assessment of relative contributions of excitatory and inhibitory metabolic activity in this structure is thus of substantial interest in psychiatric neurosciences.[3,4] In this context, mice are useful models for studying brain metabolic mechanisms associated with genetic and environmental factors influencing behavior.

Several in vivo techniques based on magnetic resonance spectroscopy (MRS) and imaging (MRI) allow to quantify metabolism underlying brain function and behavior in mice.[5,6] Amongst other, carbon-13 ($^{13}$C) MRS stands out as it allows a dynamic assessment of metabolic fluxes in vivo upon administration of a $^{13}$C-labeled substrate.[7–11] While several rodent studies have shown capability of distinguishing glial from neuronal

[1]Laboratory for Functional and Metabolic Imaging, École Polytechnique Fédérale de Lausanne, Lausanne, Switzerland
[2]Instituto de Investigaciones Biomedicas "Alberto Sols", CSIC-UAM, Madrid, Spain
[3]Sir Peter Mansfield Imaging Centre (SPMIC), School of Medicine, University of Nottingham, Nottingham, UK
[4]Center for Biomedical Imaging (CIBM-AIT), Ecole Polytechnique Fédérale de Lausanne, Lausanne, Switzerland

Corresponding authors:
Antoine Cherix, Laboratoire d'imagerie fonctionnelle et métabolique (LIFMET), EPFL, CH F0 632 (Bâtiment CH), Station 6, Lausanne CH-1015, Switzerland.
Email: antoine.cherix@epfl.ch
Hongxia Lei, Center for Biomedical Imaging (CIBM-AIT), EPFL, CH F1 627 (Bâtiment CH), Station 6, CH-1015 Lausanne, Switzerland.
Email: hongxiamri@gmail.com

contributions to total metabolic activity,[12–14] fewer studies have separated glutamatergic and GABAergic metabolism. GABAergic flux analysis in rodent brain has generally been limited to ex vivo experiments[15] or qualitative in vivo assessment of [3-$^{13}$C]-GABA formation upon $^{13}$C-labeled substrate infusion.[16–18] Quantitative analyses have generally been achieved after experimentally increasing GABA levels[19,20] or upon combined infusion of [1,6-$^{13}$C$_2$]Glc and [2-$^{13}$C] acetate.[21] Although direct $^{13}$C detection provides the best spectral resolution leading to good separation between metabolite resonances,[22,23] its very low sensitivity makes GABA detection rather difficult in rodent brains, even more so in mouse hippocampus. Alternatively, indirect $^{13}$C-MRS ($^1$H-[$^{13}$C]-MRS) has high sensitivity and studies at 9.4, 11.7 or 14 T have shown significant improvement in the detection of GABA resonances.[24–26] However, to date, experiments using $^1$H-[$^{13}$C]-MRS on mice upon $^{13}$C-glucose infusion have given only limited insight into the relative GABAergic contribution to total brain metabolism.[27–29] Among three commonly used labeled glucose, i.e. 1- 1,6- or U- (uniformly) $^{13}$C-labeled glucose (Glc), [U-$^{13}$C$_6$]Glc shows the best fitting potential in $^1$H-[$^{13}$C]-MRS spectra with its numerous visible resonances, but may be subjected to quantification bias due to unsatisfactory $^{13}$C-decoupling efficiency at 14.1 T. In fact, incomplete decoupling of [U-$^{13}$C$_6$]Glc resonances, typically observed due to RF power limitations, may affect the quantification of glucose itself, but may impact quantification of adjacent/overlapping metabolites as well.

While [1,6-$^{13}$C$_2$]Glc has often been preferred for $^{13}$C-MRS studies, as it allows the assessment of glial cells metabolic contribution when considering a two-compartment mathematical model,[30] [U-$^{13}$C$_6$]Glc produces more detectable labeling signals, and might thus lead to a better quantification of low concentrated GABA-enrichment curves, typically suited for the hippocampus. Recently, significant improvements have been achieved in the mathematical modeling of mouse brain metabolism by combining direct $^{13}$C-MRS upon infusion of [1,6-$^{13}$C$_2$]Glc with $^{18}$FDG-PET, allowing the study of neuron-glial metabolism in a small mouse brain volume.[13] So far, the benefits of such multimodal approach in mouse remain to be tested using [U-$^{13}$C$_6$] Glc infusion and using additional blood labeling analysis in order to study hippocampal metabolism.

In this study, we aimed at (1) evaluating the feasibility of including glucose spectra with three decoupling efficiencies in the basis-set for quantification; (2) seeking a new approach for modeling GABA metabolism particularly suited for $^1$H-[$^{13}$C]-MRS upon [U-$^{13}$C$_6$]Glc infusion. By combining $^{18}$FDG-PET, $^{13}$C modeling as well as high-resolution NMR experiments,

we provide a critical assessment of the feasibility of combined energetic and neurotransmission metabolic activity in mouse hippocampus.

## Methods and materials

### Animals

All experiments were carried out with the approval of the Cantonal Veterinary Authorities (Vaud, Switzerland) and conducted according to the Federal and Local ethical guidelines of Switzerland (Service de la consommation et des affaires vétérinaires, Epalinges, Switzerland) in compliance with the ARRIVE (AnimalResearch: Reporting in vivo Experiments) guidelines. Animals were housed in standard plexiglass filter-top cages in a controlled facility with temperature set at $23 \pm 1°C$ and humidity at 40%. Mice were kept in a normal 12-h daylight cycle and had ad libitum access to water and standard rodent chow diet.

### Animal preparation

Male C57BL6/J mice (N = 8) at the age of six weeks ($18 \pm 2$ g) were fasted overnight (12 h) and placed in a new cage on the evening prior to the scan. Anesthesia was induced with isoflurane at 3% (vol/vol) in a mixture of air/$O_2$ (1:1), thereafter animals were maintained at 2% isoflurane for the preparation. In particular, one femoral vein was cannulated for infusion of a 20% (m/v) [U-$^{13}$C$_6$] glucose solution during the scan (Sigma Aldrich, St Louis, MO, USA). Blood glucose concentration was measured using a Breeze-2 meter (Bayer AG, Leverkusen, Germany) before (6.9 $\pm 0.9$ mM) and after ($7.7 \pm 3.3$ mM) the preparation. The animals were then placed in a horizontal holder with the head fixed using a nose cone and two ear bars (Rapid Biomedical, Rimpar, Germany). During the 230-min scan, animals were monitored (SA Instruments Inc., New York, NY, USA) and maintained for body temperature ($36.2 \pm 0.3°C$) by circulating warm water via silicon tubes and breathing rates in the range of $78 \pm 7$ bpm by adjusting the delivery of isoflurane in the range of 1–1.5% (vol/vol). After a first 5-min bolus of glucose (3.2 mL/kg of 99% enriched $^{13}$C glucose), the infusion was maintained at a constant rate (10 mL/kg/h of 70% enriched [U-$^{13}$C$_6$]Glc) over the whole infusion time, up to 4 h. The bolus provides a means of rapidly adding labeling to the endogenous blood, mixing with the existing $^{12}$C-glucose, to reach the target FE of 70% within a few minutes, thus providing a plasma glucose isotopic enrichment time course resembling a step-function.[30] At the end of the experiment, blood glucose and lactate levels were

measured using two nearby GM7 analyzers (Analox Instruments Ltd, Stourbridge, UK).

## $^1$H-[$^{13}$C]-MRS acquisition of mouse hippocampus

Animals were scanned in a horizontal 14.1 T/26 cm magnet (Agilent Inc., USA) with a homemade $^1$H-$^{13}$C surface coil.[31] For optimal sensitivity in the bilateral dorsal hippocampus, the diameter of the $^{13}$C loop was set to 7 mm, and to 10 mm for each of the two $^1$H loops in quadrature. A set of fast-spin echo (FSE) images were acquired (TE$_{eff}$/TR = 40/2000 ms, average = 1, 15 × 0.6 mm slices, data matrix = 128 × 128, field-of-view (FOV) = 20 × 20 mm$^2$) for localizing the volume of interest (VOI). The VOI (5.5 × 2 × 1.5 mm$^3$) was placed to include both dorsal hippocampi after what field homogeneity was optimized using FAST(EST) MAP to reach a typical water linewidth of 20 ± 1 Hz, based on the full width at half maximum (FWHM).[32] $^1$H-[$^{13}$C]-MRS spectra were acquired using the full intensity SPECIAL-BISEP sequence (TE = 2.8 ms, TR = 4000 ms, averages = 8) as previously described.[28,29,33] Proton frequency offset of the inversion pulse was set at the resonance of glutamate C4 (2.34 ppm), and carbon frequency offset for the decoupling and inversion pulses was set at 45 ppm, as previously described.[28] The powers of the respective pulses were calibrated on a phantom containing an aqueous solution of [2-$^{13}$C] acetate (Sigma Aldrich, St. Louis, MO) in a voxel with similar properties (distance and size) as the in vivo hippocampus. These calibrations resulted in a bandwidth of 14 kHz (90 ppm at 14.1 T) for the inversion pulse and of 10 kHz (65 ppm at 14.1 T) for the $^{13}$C decoupling pulse. Decoupling consisted in a hyperbolic secant HS8 adiabatic full-passage[34] together with a MLEV-4 cycle and five-step phase supercycle[35] applied during the entire acquisition period (145 ms). The proton and inverted spectra (editing ON and OFF) were obtained using an interleaved acquisition and were subtracted in the post processing steps by subtracting each proton spectrum with its associated inverted counterpart to obtain the final edited spectrum containing only $^{13}$C-bound $^1$H resonances.

## $^1$H-[$^{13}$C]-MRS spectral analysis

The 16 spectra of each acquisition block were then frequency corrected and summed for quantification with LCModel resulting in one measurement time point. Both edited and non-edited spectra were quantified with LCModel. LCModel analyzes MRS data by fitting a linear combination of individual metabolite resonances, from a basis set, to the in vivo spectra, by adjusting their amplitudes, phases and linewidths.[36]

The individual metabolite spectra are generally simulated or measured in vitro and incorporated into the basis set prior to the analysis with LCModel. The non-edited proton spectra were quantified using a standard basis set including simulated mouse brain metabolite: glucose (Glc), lactate (Lac), alanine (Ala), creatine, phosphocreatine, ascorbate, glutathione, N-acetyl-aspartate, N-acetylaspartyl-glutamate, myo-inositol, scyllo-inositol, glutamate (Glu), glutamine (Gln), $\gamma$-aminobutyric acid (GABA), aspartate (Asp), taurine, glycerophosphorylcholine, choline, phosphocholine, phosphoethanolamine, as well as the measured macro-molecules (mac).[37,38] In addition, the non-edited basis set only included the coupled and decoupled component of glucose. The basis set of the edited spectra was adapted for [U-$^{13}$C$_6$]Glc infusion metabolism by including following simulated metabolite resonances in the model: LacC3, LacC2, AlaC2+C3, GluC4, GluC3, GluC2, GlnC4, GlnC3, GlnC2, AspC3, AspC2, GABAC4, GABAC3 and GABAC2. Glucose $^{13}$C resonances are highly deshielded, and to overcome quantification bias due to unsatisfactory decoupling, three decoupling efficiencies were acquired in an aqueous solution of [U-$^{13}$C$_6$]Glc during full decoupling of resonances C2-6 (dec), full coupling (coup) and partial decoupling (part; as depicted in Supplementary Figure 1(a)) and included in the basis set. The relative efficiency of the decoupling and total amount of $^{13}$C-labeled brain glucose in vivo can be calculated as follows: % Coupling = (Glc$_{coup}$/ΣGlc$_x$) × 1 + (Glc$_{part}$/ΣGlc$_x$) × 0.5; where ΣGlc$_x$ = Glc$_{coup}$ + Glc$_{part}$ + Glc$_{dec}$, i.e. the sum of the individual spectra of glucose quantified with the modified basis set (see Supplementary Figure 1 (c)). Absolute concentration of metabolites was obtained from the quantification of non-edited spectra with LCModel[36] using the water signal as internal reference assuming 80% brain water content. Fitting quality was assessed with the Cramér-Rao lower bounds errors (CRLB)[39] using a cut-off of 50%, above which quantification was assumed to be unreliable. CRLB of the labeled resonances reported in the results were calculated from the second half of the infusion, to represent steady-state values. Correlation of the different peak intensities, spectral SNR and linewidth are reported as given by LCModel. Isotopic fractional enrichment (FE) was calculated for each metabolite by dividing the labeled atom signal over the metabolite concentration as described previously.[27] Finally, the FE curves were multiplied by the metabolite concentration to obtain the metabolic $^{13}$C-enrichment curves, which were then averaged for all the animals and used for the proposed metabolic models, described in the following sections.

## FE measurements of blood glucose, acetate and acetate

The enrichments of blood glucose, lactate and acetate were measured in a subgroup of three animals which underwent surgery and [U-$^{13}C_6$]Glc infusion without any scan. Retro-orbital blood collection was performed at three different time points (20, 60 and 180 min after glucose infusion start) with lithium/heparin Microvette collection tube (Sarstedt AG, Nümbrecht, Germany). Blood was then centrifuged for 2 min at room temperature (6 000 r/min) to extract the plasma which was then frozen in liquid nitrogen. Blood metabolites were subsequently extracted using a chloroform/methanol extraction protocol followed by lyophilization.[40] Metabolites were then resuspended in deuterium oxide containing 0.1 mM DSS (4,4-dimethyl-4-silapentane-1-sulfonic acid) as internal reference. High resolution $^1H$-NMR (HR-NMR) was performed on the samples with a DRX-600 spectrometer (Bruker BioSpin, Fällanden, Switzerland) using a pulse acquired $^1H$ sequence (flip angle $= 30°$, pulse delay $= 5s$, acquisition time $= 2.7s$, number of acquisitions $= 160$). FE was calculated based on the resonances of $\beta$-Glc H6, Lac H3 and acetate H3, bound to $^{13}C$ and $^{12}C$ respectively. Based on their respective coupling constants (Glc $J_{C-H}(\beta$-H1): 169 Hz, Lac $J_{C-H}$(H3): 131 Hz, Acetate $J_{C-H}$(H3): 130 Hz), the coupled and uncoupled proton resonances ([$^1H$-$^{12}C$] and [$^1H$-$^{13}C$]) were integrated, normalized, and calculated into the corresponding metabolite FE.

## $^{18}FDG$ positron emission tomography and cerebral metabolic rate of glucose

In vivo measurements of cerebral glucose uptake were performed on a different group of animals (N = 3, not fasted) with positron emission tomography (PET) as previously described in detail.[41] Briefly, catheter insertion of the tail vein was performed under 2% (vol/vol) isoflurane anesthesia, allowing for substrate administration, and blood sampling to establish initial and final glycemia values. Mice were prone positioned on a heat-regulated scanner bed to accommodate: (1) insertion of a respiratory cushion between the thorax and the bed; (2) insertion of a rectal thermometer; and (3) delivery of isoflurane via a nose mask. Animals were positioned with the thoracic region in the center of the field of view, allowing the inferior vena cava (the anatomical source of the input function) and brain (hippocampus) to be imaged simultaneously. During the 50-min scan, mice were maintained under 1–1.5% (vol/vol) isoflurane anesthesia in oxygen. Monitored temperature and breathing rate were maintained within a physiological range. PET coincidence data were acquired in list mode (see below) and coordinated with the i.v. bolus injection of $^{18}F$-fluorodeoxyglucose ($^{18}FDG$) ($\sim$50 MBq) through the tail vein catheter within the first 20 s of the PET scan, followed by 50–200 $\mu$L of saline chase solution. Imaging was performed using an avalanche photodiode-based small animal micro-PET scanner (LabPET4; Gamma Medica, Sherbrook, Canada). Prior to image reconstruction, list mode data were histogrammed using the following number of frames (F) and frame duration (s): 24 F, 5 s; 6 F, 30 s; 5 F, 2 min; 7 F, 5 min. After image reconstruction with the Labpet software, PMOD 2.95 software (PMOD Technologies, Zurich) was used for the determination of the standardized uptake value (SUV), defined as (mean ROI activity [kBq/cm$^3$])/(injected dose [kBq]/body weight [g]). Regions of interest, i.e. hippocampus ($2 \times 5.5$ mm$^2$), were manually drawn over one axial slice. Mathematical modeling of hippocampal glucose metabolism was performed as previously described[41] using the activity density (Bq/cm$^3$) corrected for the decay at the initial scan time. Briefly, glucose kinetic parameters were obtained from a Sokoloff model description of FDG metabolism with four parameters pools using the activity measured in the vena cava as the input function and the tissue activity from the hippocampus (including 3% partial blood volume). The blood glucose concentration (Cp) was the value obtained from the tail vein at the end of the PET experiment and the lumped constant (LC) was fixed to 0.6. The adjusted metabolic parameters were: the transport constants between blood and hippocampus (k1 and k2), phosphorylation constants (k3 and k4) and CMR$_g$ (calculated as (Cp/LC) $\cdot$ k1 $\cdot$ k3/(k2+k3)).

## One-compartment modeling of hippocampal metabolic fluxes

A simple one-compartment model was taken from Xin et al.[27] and modified with additional information. In brief, pyruvate C3 is labeled from [U-$^{13}C_6$]Glc and enters brain TCA cycle, which labels aspartate and glutamate through the transmitochondrial flux. The labeling of glutamine arises from neurotransmission cycling and exchanges with the glutamate pool. Mathematical modeling of the data acquired from $^1H$-[$^{13}C$]-MRS was complemented with FE measurements of plasma lactate/acetate from high-resolution NMR and CMR$_g$ determined from PET. A thorough description of the model is provided in the Supplementary Material and Figure 1(a).

To estimate the hippocampal metabolic fluxes, the measured $^{13}C$-labeling curves, i.e. Glc, LacC3, GluC4, GluC3, GlnC4, GlnC3 and AspC3, were fitted in the proposed one-compartment model using a standard
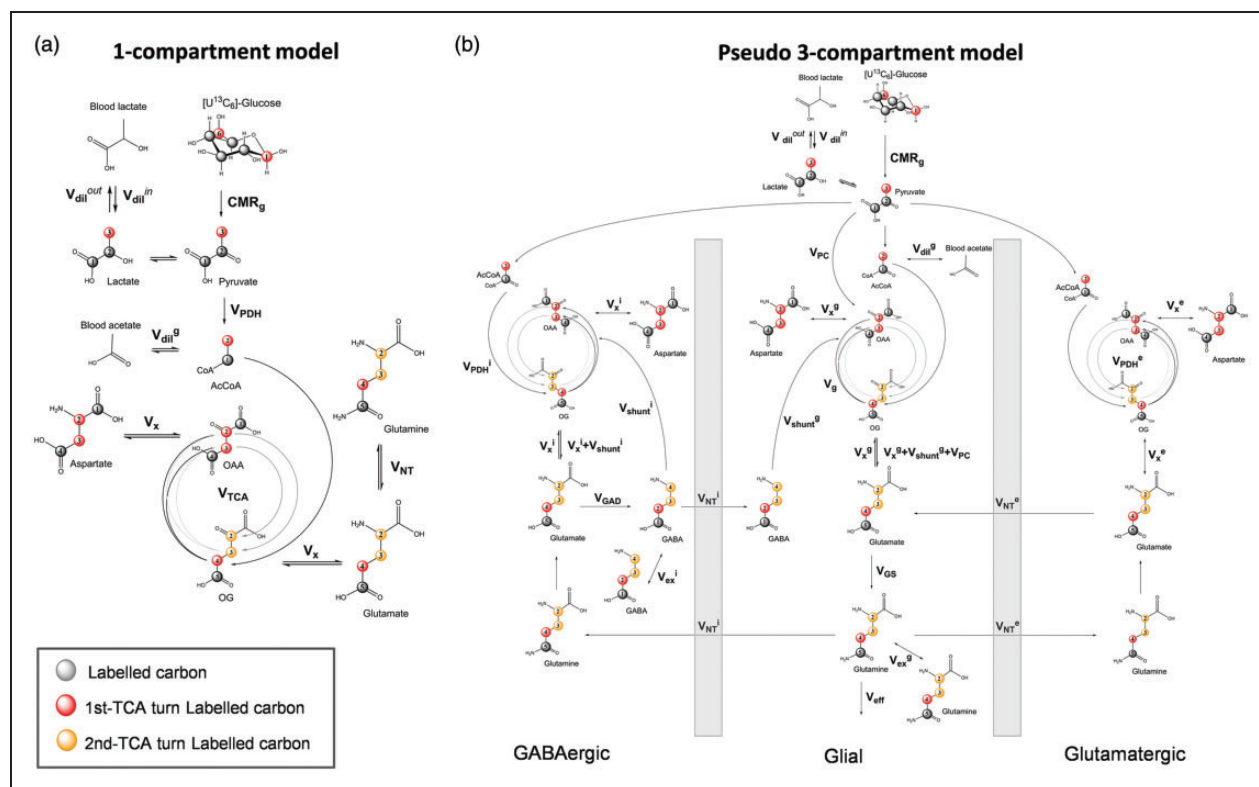
**Figure 1.** Mathematical models of hippocampal metabolism. (a) Scheme of the one-compartment model of hippocampal brain metabolism used to fit the ^{13}C enrichment curves, including: pyruvate dehydrogenase activity ($V_{PDH}$), tricarboxylic acid cycle ($V_{TCA}$), a dilution flux from blood lactate ($V_{dil}^{in}$ and $V_{dil}^{out}$) and from blood acetate ($V_{dil}^{g}$), a transmitochondrial flux ($V_x$) and a neurotransmission flux ($V_{NT}$). (b) Scheme of the pseudo three-compartment model of brain metabolism compartment model used to fit the ^{13}C enrichment curves. Fluxes are separated into glutamatergic ($^e$), GABAergic ($^i$) and glial ($^g$) compartments. Cerebral metabolic rate of glucose ($CMR_g$), pyruvate dehydrogenase activity ($V_{PDH}$), glial tricarboxylic acid cycle ($V_g$), a dilution flux from blood lactate ($V_{dil}^{in}$ and $V_{dil}^{out}$) and from blood acetate ($V_{dil}^{g}$), a transmitochondrial flux ($V_x$), a neurotransmission flux ($V_{NT}$), pyruvate carboxylase flux ($V_{PC}$), a Gln efflux ($V_{eff}$), glutamine synthetase activity ($V_{GS}$), glutamate decarboxylase activity ($V_{GAD}$), GABA TCA shunt ($V_{shunt}$) and two exchange fluxes between two Gln or two GABA pools ($V_{ex}^{g}$ and $V_{ex}^{i}$).

built-in ordinary differential equation solver together with a modified Levenberg–Marquardt nonlinear weighed regression method using MATLAB (Version 8.3, The MathWorks, Inc., Natick, MA). Glucose FE curve was used as an input function for both models and was fitted with an inverse exponential function with an oblique asymptote (a·t + b)·(1 − exp(−c·t)). A weighing based on the relative CRLB of each ^{13}C metabolite resonance was used for each labeling curve in the regression cost function. Precision of the metabolic fluxes was further evaluated with Monte Carlo simulations (300 artificial turnover curves) providing a flux probability distribution.[11]

## Pseudo three-compartment modeling of hippocampal metabolic fluxes

The pseudo three-compartment model was adapted from Duarte and Gruetter[26] to resemble the reality of brain cell-specific metabolism and particularly the differences between glutamatergic (excitatory) and GABAergic (inhibitory) neurons. Since uniformly labeled glucose does not differentiate ^{13}C labeling produced by the pyruvate carboxylase (PC), all glial fluxes were then taken from the literature. In particular, the PC flux ($V_{PC}$) was set to 0.04 μmol/l/min,[13,28] glial TCA cycle was set to $V_g = 0.16$ μmol/l/min[13] and the glial transmitochondrial flux ($V_x^g$) was set to be equal to $V_g$.

Since the presence of a multiple glial Gln pools in astrocytes has been described,[42] and shown to improve fitting of experimental data with a three-compartment model,[26] we propose a similar approach with the addition of a pool for GABAergic neurons. Including two GABA pools is closer to the biochemical reality underlying the function of the two GAD isoforms, one being more cytoplasmic (GAD67) and the other being neurotransmission-related (GAD65).[43] GAD activities are very heterogeneous and highly regulated; however, for simplification purpose, relative GABA pools were

set to relative GAD concentrations in the mouse hippocampus, i.e. a 1:1 relation for both isoforms.[44] Overall, $CMR_g$, $V_{dil}^{in}$, glutamatergic fluxes $V_{PDH}^e$, $V_x^e$, $V_{NT}^e$, GABAergic fluxes $V_{PDH}^i$, $V_x^i$, $V_{NT}^i$, glutamate decarboxylase activity ($V_{GAD}$), as well as two exchange fluxes $V_{ex}^g$ and $V_{ex}^i$ reflecting the presence of two Gln pools in glia as well as two GABA pools in inhibitory neurons, were included. The superscripts of e, i and g indicate glutamatergic, GABAergic and glial compartments, respectively. In addition to Glc, LacC3, GluC4, GluC3, GlnC4, GlnC3 and AspC3 ^{13}C-labeling curves used for one-compartment model and the NMR and PET data, GluC2, GlnC2, GABAC2, GABAC3 and GABAC4 were included in the pseudo three-compartment model. More details of the equations describing the mathematical models used are given in the Supplementary Material and Figure 1(b).

### Statistics

Correlations were performed using GraphPad Prism (GraphPad software, San Diego, CA, USA). All values are given as mean $\pm$ SD. Statistical tests were performed using unpaired Student $t$-tests with significance set at $p < 0.05$.

## Results

### ^{1}H-[^{13}C]-MRS of mouse dorsal hippocampus at 14 Tesla

At the end of the glucose infusion, blood glucose reached a concentration of $20.8 \pm 4.1$ mM and blood lactate level post-infusion was $7.9 \pm 2.4$ mM. Resulting ^{1}H-[^{13}C]-MRS spectra (16 times 8 average blocks) led to a time resolution of about 10 min for every metabolite (Figure 2(a)). Quantification of the non-edited spectra with LCModel (Figure 2(b)) provided hippocampal metabolite concentrations used for the modeling, i.e. Glu $= 6.4 \pm 1.0$ mM, Gln $= 2.6 \pm 0.5$ mM, Asp $= 1.0 \pm 0.1$ mM, and GABA $= 1.7 \pm 0.6$ mM. Lactate levels were relatively stable and low ($2.5 \pm 0.9$ mM) with an increase of only 0.2 mM from the initial value towards the end of the infusion. The SNR of the non-edited spectra was $21 \pm 1$ with a linewidth of $17 \pm 2$ Hz as calculated by LCModel. For the edited spectra, the SNR was $7 \pm 2$ over the whole infusion time course ($5 \pm 2$ in the first half of the protocol, $8 \pm 1$ in the second).

### Spectral fitting results

The inclusion of glucose spectral patterns with three different decoupled efficiencies in the basis set (Supplementary Figure 1) improved the quantification of glucose and GABAC4, i.e. with reduced average CRLB of Glc $= 3.4 \pm 0.7\%$ (from $5.1 \pm 3.7\%$) and GABAC4 $= 18 \pm 4\%$ (from $110 \pm 318\%$, Supplementary Figure 2). Average CRLBs for the other resonances were largely not affected, i.e.: LacC3 $= 5 \pm 1\%$, GluC4 $= 3.1 \pm 0.4\%$, GluC3 $= 6.8 \pm 1.5\%$, GluC2+GlnC2 $= 20 \pm 11\%$, GlnC4 $= 8 \pm 1\%$, GlnC3 $= 12 \pm 2\%$, AspC3 $= 28 \pm 6\%$, GABAC2 $= 26 \pm 7\%$ and GABAC3 $= 21 \pm 5\%$. The correlation matrix resulting from the different resonance fitting by LCModel indicated that GluC3 and GlnC3 were relatively less correlated than usual (R $= -0.73$) while GluC2 and GlnC2 were highly dependent (R $= -0.85$; Supplementary Figure 2(a)).

### Quantification results of metabolic fractional enrichment in mouse hippocampus and blood

As shown in Figure 3(a), the FE of hippocampal Glc reached a plateau in a near step function to $0.70 \pm 0.10$ that was faster than both FEs of hippocampal Lac ($0.62 \pm 0.07$) and GluC4 ($0.52 \pm 0.05$; Figure 3(a)) but similar to that of blood Glc, i.e. $\sim 0.7$ (Figure 3(b)). The FE of blood Lac reached a plateau at $\sim 0.5$ but not that of blood acetate (Figure 3(b)). In hippocampus, GlnC4 FE reached a plateau after 150 min at $0.47 \pm 0.09$, while around 180 min, FEs of GluC3, GlnC3 and GlxC2 reached their respective steady state, i.e. $0.53 \pm 0.08$, $0.47 \pm 0.05$ and $0.43 \pm 0.17$. In addition, all the GABA enrichment curves showed rapid labeling patterns and reached steady-state around 150 min for GABAC2 and 180 min for GABAC3 and 4. The FEs of GABAC2-4 at steady state were not significantly different from each other ($p > 0.05$), i.e. $0.32 \pm 0.08$ for GABAC2, $0.37 \pm 0.08$ for GABAC3 and $0.34 \pm 0.04$ for GABAC4. Finally, AspC3 showed the highest variability in the labeling but reached a plateau around 150 min at $0.49 \pm 0.17$. The accumulation curves of [18]FDG during the PET experiments (Figure 3(c)) were reproducible and modeling of glycolytic flux led to a cerebral metabolic rate of $CMR_g = 0.61 \pm 0.02$ µmol/g/min. The other [18]FDG rate constants obtained were as follows: k1 $= 0.39 \pm 0.08$ min$^{-1}$, k2 $= 0.57 \pm 0.11$ min$^{-1}$, k3 $= 0.06 \pm 0.02$ min$^{-1}$, k4 $= 0.04 \pm 0.02$ min$^{-1}$.

### Mathematical modeling of hippocampal metabolism

The one-compartment model of glucose metabolism (Figure 1(a)) generated a satisfactory fit of the data (Figure 4) with no strong flux correlation (i.e. <0.8; Supplementary Figure 3(a)). The resulting metabolic fluxes are summarized in Table 1. For instance, we measured a TCA cycle ($V_{TCA}$) of
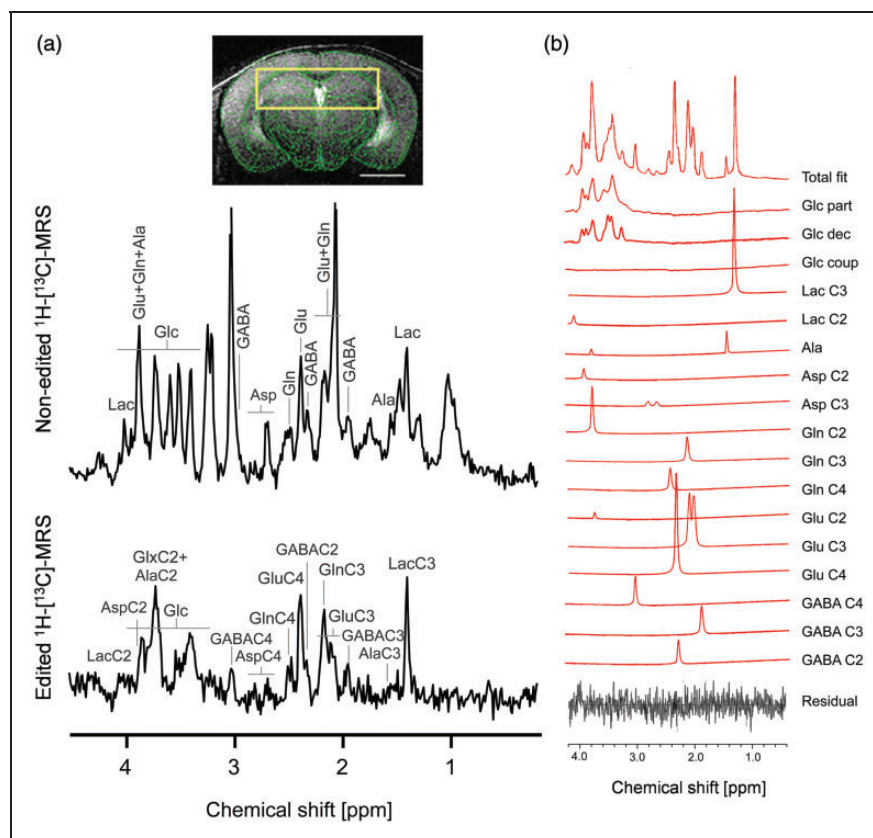
**Figure 2.** $^1$H-[$^{13}$C]-MRS in mouse dorsal hippocampus. (a) Typical non-edited ($^{12}$C+$^{13}$C, top) and edited ($^{13}$C, bottom) $^1$H-[$^{13}$C]-MRS spectra acquired from mouse hippocampus (yellow box in one MR image; scale bar = 2mm) after 3 h of [U-$^{13}$C$_6$]Glc infusion. Labeling of relevant metabolites is indicated: Lactate (Lac), glutamate (Glu), glutamine (Gln), alanine (Ala), γ-aminobutyric acid (GABA) and aspartate (Asp). In the edited spectrum, the carbon position number coupled with the observed proton resonance is indicated for each metabolite. (b) Example of fitting the edited spectrum with LCModel using a basis set corrected for glucose coupling, i.e. including partially decoupled (Glc part), decoupled (Glc dec) and coupled (Glc coup) glucose (More details in Supplementary Figure 1). In this example, very minimal Glc coup was detected by the LCModel.

$1.71 \pm 0.03 \, \mu mol/g/min$ and a neurotransmission rate ($V_{NT}$) of $0.062 \pm 0.006 \, \mu mol/g/min$. Our 1-compartment approach was extended to include GABA metabolism, as adapted from a previous model of hypothalamic metabolism[28]; however, resulting GABA metabolic rates remained unreliable.

The proposed three-compartment model of glucose metabolism (Figure 1(b)) provided overall satisfactory fits on the $^{13}$C-labeling curves of LacC3, GluC3-4, GlnC3-4, AspC3, and GABAC2-4 ($R^2 = 0.988$; Table 2 and Figure 5), with limited number of correlations between fluxes (the absolute coefficients of four parameters were >0.7; Supplementary Figure 3(b)) and coherence of flux results. Importantly, the addition of a second GABAergic GABA pool (Supplementary Figure 4(a)) and a second astrocytic Gln pool (Supplementary Figure 4(b)) improved the overall fitting (total goodness-of-fit $R^2$ value) by 0.6% and 0.4%, respectively, as compared to the 1-pool models. The summary of the estimated

fluxes is reported in Table 2. Since the glial metabolic rates were taken from the literature, due to the fact that [U-$^{13}$C$_6$]Glc does not assess astrocyte metabolism reliably, varying these values in a ±100% range resulted only in an approximately ±25% difference in the estimation of main fluxes (Supplementary Figure 3(c)).

## Discussion

This study shows for the first time that a metabolic flux analysis of mouse hippocampal glucose metabolism is feasible in mouse brain in vivo using $^1$H-[$^{13}$C]-MRS and $^{18}$FDG-PET to distinguish glutamatergic and GABAergic neuron activity. With improved glucose quantification and a more sophisticated mathematical model including two separate GABA pools and a second glial Gln pool, we have been able to assess the relative metabolic contributions of
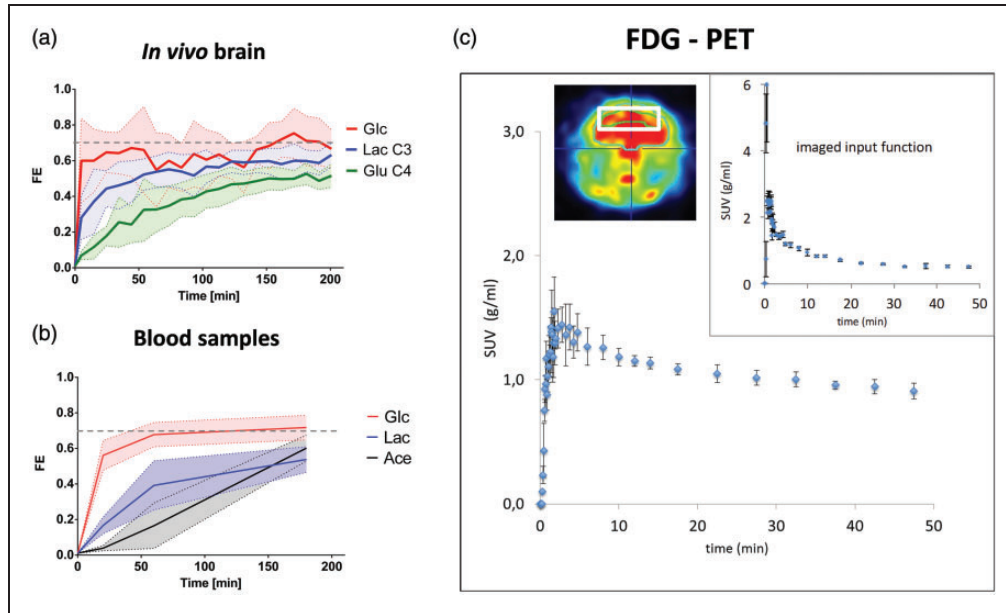
**Figure 3.** Glucose labeling in hippocampus and plasma during $^1$H-[$^{13}$C]-MRS. (a) Averaged fractional enrichment (FE) of brain glucose (Glc), lactate C3 (Lac C3) and glutamate C4 (Glu C4) during the in vivo MRS experiment. (b) Blood plasma FE of glucose, lactate and acetate measured during [U-$^{13}$C$_6$]Glc infusion (N = 3). Shaded areas represent the SD. (c) Glucose standard uptake value (SUV) in hippocampus and vena cava input function (upper right) measured by $^{18}$FDG PET (N = 3). The heat map depicts a PET image acquired at steady-state, i.e. during the last minutes of the 50-min scan, and shows regions of high (red) and low (blue) phosphorylation of $^{18}$FDG. The voxel used for PET modeling (white box) had similar dimensions as for the $^1$H-[$^{13}$C]-MRS (i.e. 5.5 × 2 × 1.5 mm$^3$) and is shown in white on the heat map.
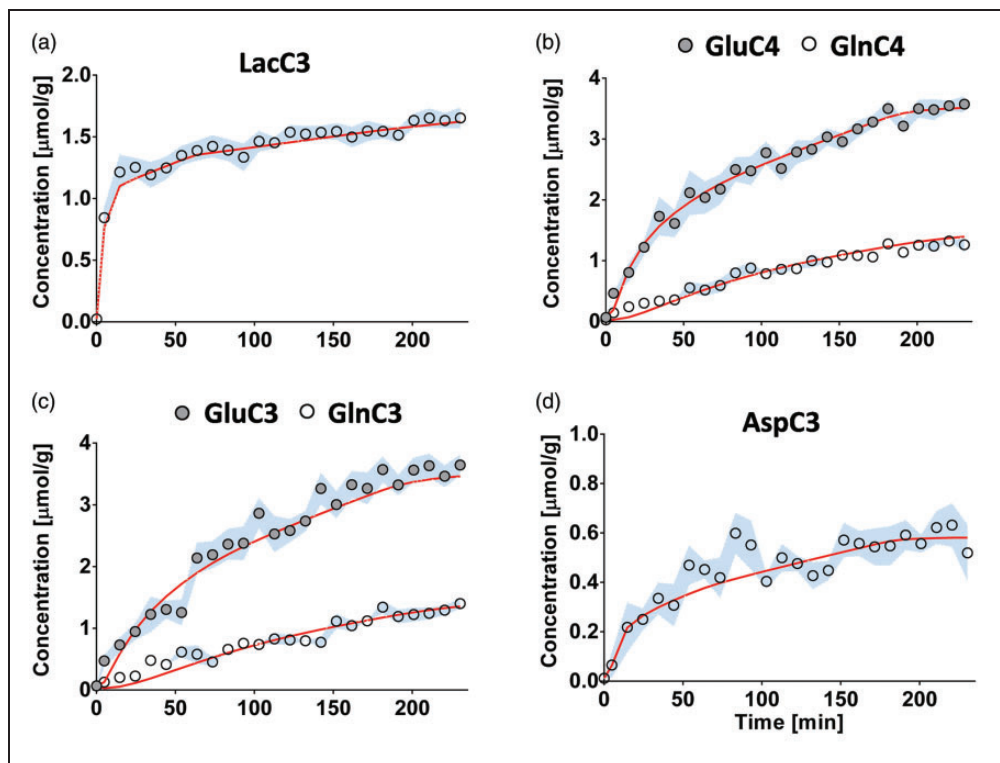


**Figure 4.** Fitting results using a one-compartment model of hippocampal metabolism. Results of the fitting of the one-compartment model (red) to the $^{13}$C enrichment curves of (a) lactate C3, (b) glutamate and glutamine C4, (c) glutamate and glutamine C3 and (d) aspartate C3, shown as the mean for all animals (circles) ± SD (blue).

**Table 1.** Flux estimation obtained with the one-compartment model compared to relevant literature

|  | Current study<br>*Mouse/isoflurane* | Xin et al.[27]<br>*Mouse/isoflurane* | Lizarbe et al.[29]<br>*Mouse/isoflurane* | Lai et al.[13]<br>*Mouse/isoflurane* |
|---|---|---|---|---|
| One-compartment model |  |  |  |  |
| $R^2$ | 0.988 | $^1$H-[$^{13}$C]-MRS/<br>[U-$^{13}$C$_6$]Glc | $^1$H-[$^{13}$C]-MRS/<br>[1,6-$^{13}$C$_2$]Glc | $^{13}$C-MRS/<br>[1,6-$^{13}$C$_2$]Glc |
| *CMRg fixed* | + | Lactate IF | Lactate IF | + |
| $V_{dil}^{in}$ | 0.64 ± 0.03 | – | – | – |
| $CMR_g$ | 0.61 | – | – | 0.4 |
| $V_{TCA}$ | 1.71 ± 0.03 | 1.05 ± 0.04 | 0.83 ± 0.05 | 0.16 ± 0.03 ($V_g$)<br>+ 0.56 ± 0.03 ($V_{TCA}^n$) |
| $V_x$ | 0.48 ± 0.26 | 0.48 ± 0.02 | 0.68 ± 0.21 | 0.18 ± 0.02 |
| $V_{NT}$ | 0.062 ± 0.006 | 0.20 ± 0.02 | 0.41 ± 0.07 | 0.084 ± 0.008 |
| $V_{dil}^g$ | 0.64 ± 0.21 | – | 0.06 ± 0.01 | 0.23 ± 0.05 |
| $V_{GABA}$ | – | – | 0.13 ± 0.01 | – |
| $V_{PC}$ | – | – | 0.04 ± 0.01 | 0.041 ± 0.003 |
| Calculated fluxes |  |  |  |  |
| $V_{dil}^{out}$ | 0.56 ± 0.01 | – | – | 0.20 ± 0.02 |

Note: Fluxes include: the cerebral metabolic rate of glucose ($CMR_g$), tricarboxylic acid cycle ($V_{TCA}$), a dilution flux from blood lactate ($V_{dil}^{in}$ and $V_{dil}^{out}$) and from blood acetate ($V_{dil}^g$), a transmitochondrial flux ($V_x$) and a neurotransmission flux ($V_{NT}$), pyruvate carboxylase flux ($V_{PC}$), a GABA flux ($V_{GABA}$). All fluxes are expressed in $\mu$mol/g/min. IF: input function. Values shown without "±" represent fixed values in the modeling.

excitatory and inhibitory neurons from in vivo mouse hippocampus.

## Optimization of glucose quantification improves data analysis for a [U-$^{13}$C$_6$]Glc infusion

We first incorporated the glucose spectral patterns with three decoupling efficiencies in the basis set (Supplementary Figure 1) to circumvent plausible RF limitations, which may often arise from the very broadband $^{13}$C-decoupling during $^1$H-[$^{13}$C]-MRS experiments. The quantification of both glucose and its neighboring resonance GABAC4 was noticeably improved (Supplementary Figure 2(b)). In particular, the resulting FE of hippocampal glucose was similar to that of blood glucose (Figure 3(a) and (b)), and thus could be used as an input function for the mathematical model. This is a significant improvement, as lactate has been generally preferred for that purpose in $^1$H-[$^{13}$C]-MRS experiments in mice.[27,28] The input function provides knowledge about the kinetics and labeling of the infused substrate, which is fundamental in determining the downstream metabolic rates.[30] The use of brain glucose as input function provides thus a more complete description of glucose metabolism that is upstream of mitochondria, i.e. by considering $CMR_g$ and brain/blood lactate exchange into the model.

## One-compartment modeling of mouse hippocampus

Improving FEs of both glucose and GABA, taking together $CMR_g$ from PET and the FEs of blood Lac and acetate, permits to assess neuronal metabolism with a more detailed mathematical model than previously applied in mice.[27] For instance, the proposed one-compartment model of hippocampal metabolism, which does not include GABA (Figure 1(a)), was evaluated and provided an excellent fit (i.e. $R^2 = 0.988$) for LacC3, GluC4, GlnC4, GluC3, GlnC3 and AspC3 (Table 1 and Figure 4). When compared to other mouse studies using a one-compartment model and isoflurane anesthetic, our results indicate a higher $V_{TCA}/V_{NT}$ ratio (~28) than reported by Xin et al.[27] (~5), Lai et al.[13] (~9) and Lizarbe et al.[28] (~2), which may reflect a specificity of the hippocampus (Table 1). When all FEs of GABAC2-4 were incorporated into the one-compartment model as proposed by Lizarbe et al.,[28] the overall fit outcomes did not agree with our data (data not shown). When examining the labeling of GABA, it appears that our data do not resemble a sigmoid function as seen in other studies.[24,28] Rather, the labeling curves of GABA had a steep slope and reached a steady-state quickly as seen in Duarte and Gruetter[26] and Xin et al.[27] (Figure 5). When we increased the SNR of GABA by reducing the temporal resolution, the steep slopes of GABA remained similar to the high temporal resolution ones and to Xin et al.[27] as well. Due to its direct interaction with GluC4, and fewer number of TCA turns needed to enter this position, GABAC2 is normally labeled faster than the other carbon positions. A major difference between [U-$^{13}$C$_6$]Glc and [1,6-$^{13}$C$_2$]Glc infusion is that the latter does not produce pyruvate C2 labeling,

**Table 2.** Flux estimation obtained with the pseudo three-compartment model compared to relevant literature.

GABAergic compartmentalized models

| model | Pseudo three-compartment | Three-compartment | | Three-compartment |
|---|---|---|---|---|
| | *Current study* <br> *Mouse/isoflurane* | *Duarte and Gruetter*[26] <br> *Rat/α-chloralose* | | *Patel et al.*[15] <br> *Rat/halothane*[†] <br> *Rat/pentobarbital*[§] <br> *Mason et al.*[52‡] <br> *Rat/halothane* <br> *Van Eijsden et al.*[24#] <br> *Rat/N₂O:O₂* |
| $R^2$ | 0.98 | 0.972 | 0.976 | |
| *Gln pools* | 2 | 1 | 2 | |
| *GABA pools* | 2 | 1 | 1 | |
| $V_{dil}^{in}$ | $0.73 \pm 0.23$ | – | – | |
| $CMR_g$ | 0.61 | 0.52 | 0.52 | |
| $V_{PDH}^{e}$ | $1.01 \pm 0.09$ | $0.36 \pm 0.01$ | $0.33 \pm 0.01$ | $0.98 \pm 0.02^{†}/0.28 \pm 0.12^{§}$ <br> $/ 0.472 \pm 0.040^{#}$ |
| $V_x^{e}$ | $0.081 \pm 0.007$ | $0.41 \pm 0.02$ | $0.39 \pm 0.02$ | |
| $V_{NT}^{e}$ | $0.01 \pm 0.005$ | $0.16 \pm 0.01$ | $0.18 \pm 0.01$ | $0.44 \pm 0.01^{†}/{<}0.01 \pm 0.01^{§}$ <br> $/ 0.274 \pm 0.023^{#}$ |
| $V_{PDH}^{i}$ | $0.05 \pm 0.05$ | $0.024 \pm 0.005$ | $0.017 \pm 0.005$ | |
| $V_x^{i}$ | $0 \pm 0.0$ | $0.0067 \pm 0.0038$ | $0.0068 \pm 0.0034$ | |
| $V_{NT}^{i}$ | $0.0007 \pm 0.0006$ | $0.044 \pm 0.002$ | $0.053 \pm 0.003$ | $0.13 \pm 0.01^{†}/{<}0.01 \pm 0.01^{§}$ <br> $/ 0.033 \pm 0.005^{#}$ |
| $V_{GAD}$ | $0.32 \pm 0.06$ | $0.098 \pm 0.003$ | $0.11 \pm 0.01$ | $0.25^{†}/ 0.10\text{-}015^{‡}$ |
| $V_{dil}^{g}$ | $0 \pm 0.0$ | $1.1 \pm 0.1$ | $0.76 \pm 0.07$ | |
| $V_{ex}^{g}$ | $0.024 \pm 0.005$ | – | $0.060 \pm 0.008$ | |
| $V_{ex}^{i}$ | $0.0008 \pm 0.0007$ | – | – | |
| *Calculated fluxes* | | | | |
| $V_{TCA}^{i}$ | $0.37 \pm 0.04$ | $0.077 \pm 0.007$ | $0.070 \pm 0.007$ | $0.21 \pm 0.02^{†}/0.06 \pm 0.02^{§}$ <br> $/0.062 \pm 0.009^{#}$ |
| $V_{TCA}^{g}$ | $0.200 \pm 0.001$ | $0.38 \pm 0.02$ | $0.44 \pm 0.03$ | $0.144 \pm 0.025^{#}$ |
| $V_{GS}$ | $0.045 \pm 0.005$ | $0.28 \pm 0.01$ | $0.33 \pm 0.01$ | |
| $CMR_g^{(ox)}$ | $0.85 \pm 0.06$ | $0.44 \pm 0.02$ | $0.47 \pm 0.02$ | |
| $V_{shunt}^{i}$ | $0.32 \pm 0.06$ | $0.054 \pm 0.004$ | $0.053 \pm 0.005$ | $0.025 \pm 0.006^{#}$ |
| $V_{dil}^{out}$ | $0.23 \pm 0.06$ | $0.16 \pm 0.03$ | $0.11 \pm 0.03$ | |
| $V_x^{g}$ | 0.16 | $0.010 \pm 0.011$ | $0.018 \pm 0.018$ | |

Note: Estimated fluxes include: the cerebral metabolic rate of glucose ($CMR_g$), pyruvate dehydrogenase activity ($V_{PDH}$), an influx from blood lactate ($V_{dil}^{in}$) and a dilution flux from blood acetate ($V_{dil}^{g}$), a transmitochondrial flux ($V_x$), a neurotransmission flux ($V_{NT}$), glutamate decarboxylase activity ($V_{GAD}$), and two exchange fluxes between two glial Gln or two GABA pools ($V_{ex}^{g}$ and $V_{ex}^{i}$). Calculated fluxes include: the oxidative cerebral metabolic rate of glucose ($CMR_g$(ox)), GABA TCA shunt ($V_{shunt}$), Glutamine synthetase activity ($V_{GS}$) and an efflux from blood lactate ($V_{dil}^{out}$), total GABA TCA is $V_{TCA}^{i} = V_{PDH}^{i} + V_{shunt}^{i}$; and total glial TCA is $V_{TCA}^{g} = V_g + V_{PC} + V_{NT}^{i}$. Excitatory compartment ($^e$); inhibitory compartment ($^i$); glial compartment ($^g$). All fluxes are expressed in $\mu mol/g/min$. IF: input function. Values shown without "$\pm$" represent fixed values in the modeling.
[†]Patel et al.[15] using rats under halotane anesthesia.
[§]Patel et al.[15] using rats under pentobarbital anesthesia.
[‡]Mason et al.[52] using rats under halothane anesthesia.
[#]Van Eijsden et al.[24] using rats under N₂O:O₂ anesthesia.

thus leading to the dilution of GluC3 and GlnC3 pools, as compared to their C2 equivalents, through the activity of glial pyruvate carboxylase. As a result, with [U-¹³C₆]Glc, GABAC3 labeling pool, arising from GluC3, is not diluted and reaches similar levels as GABAC4, providing better detection and quantification than when [1,6-¹³C₂]Glc is used. Although we cannot exclude that this GABA labeling differing from that of hypothalamus[28] is due to regional difference, it is likely to be related to the use of [U-¹³C₆]Glc as well.

## Compartmentalized modeling of brain excitatory/inhibitory metabolic balance using a pseudo three-compartment metabolic flux analysis

Then a more complex pseudo three-compartment model, including GABAergic, glutamatergic and glial
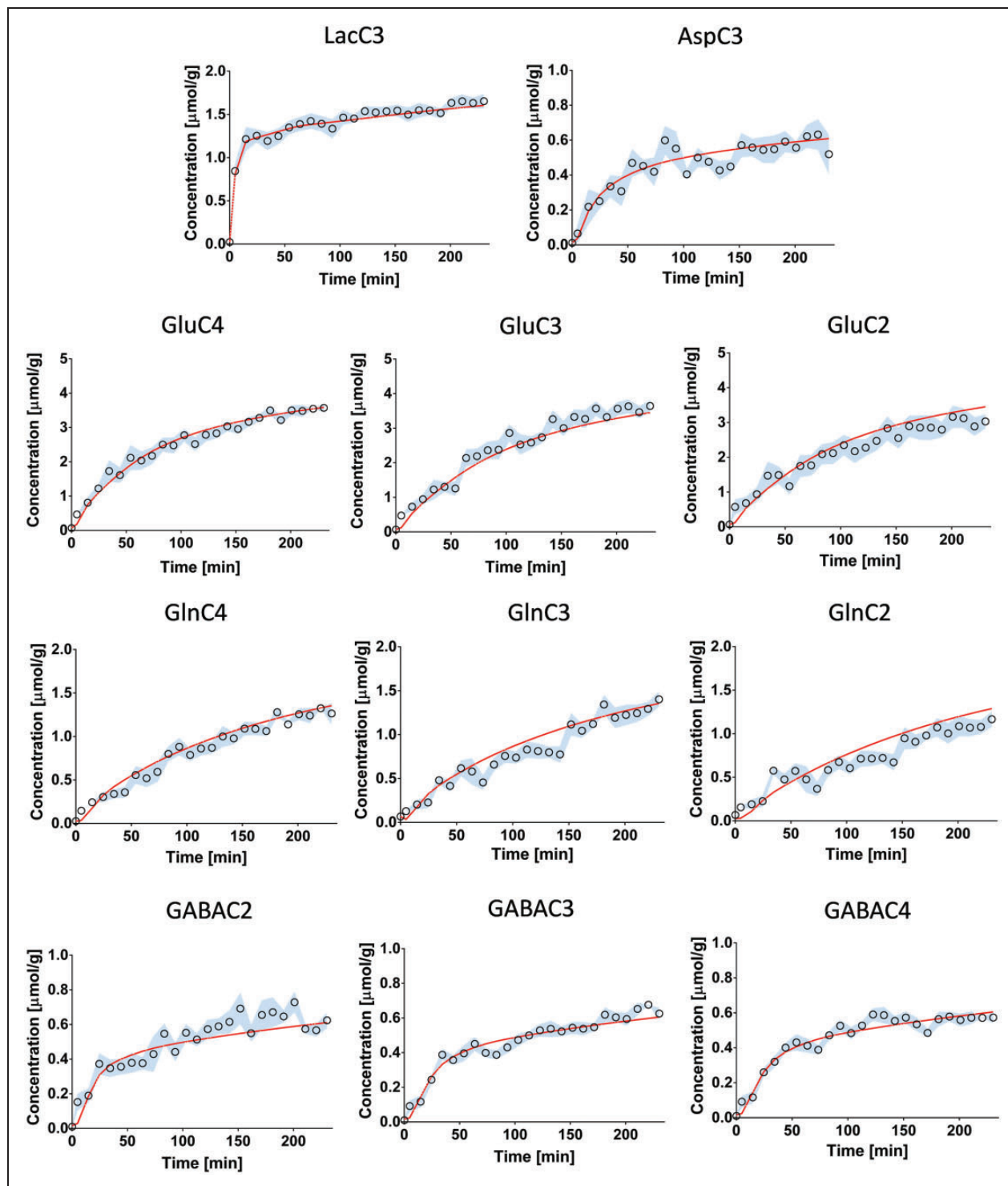
**Figure 5.** Fitting results using a pseudo three-compartment model of hippocampal metabolism. Results of the fitting of the pseudo three-compartment model (red) to the ^{13}C-enrichment curves (circles), shown as the mean for all animals ± SD (blue).

compartments was explored. In particular, the inclusion of GABA labeling curves for this cell-specific metabolism description of the brain led to some additional observations when compared to the one-

compartment model: Duarte and Gruetter[26] have reported that the addition of GABAergic metabolism increased the total $CMR_g(ox)$ compared to a glia-neuronal two-compartment model. This effect has

been proposed to arise from the glial recycling of GABA, leading to a higher glial TCA cycle ($V_{TCA}^g$). In the present study, the addition of GABA labeling in our model did not induce a rise in the total $V_{TCA}$, rather, inclusion of GABA (and fixed glial fluxes) resulted in a very similar mitochondrial oxidation: $V_{TCA} = 1.71 \pm 0.03\,\mu mol/g/min$ in the one-compartment model versus $V_{TCA}$ ($= 2 \times CMR_g(ox)) = 1.70 \pm 0.12\,\mu mol/g/min$ in the pseudo three-compartment model (Tables 1 and 2). This difference could arise from the difference in how blood/brain lactate kinetics are modeled here, and the net lactate influx in the hippocampus ($V_{dil}^{in} - V_{dil}^{out}$) is likely to influence $CMR_g(ox)$. In fact, when compared to the glia-neuronal two-compartment model after infusion of $[1,6^{-13}C_2]Glc$ presented in Lai et al.,[13] our analysis reveals much higher levels of TCA cycle activity ($+137\%$; $V_{TCA}$ in the one-compartment model here versus $V_g + V_{TCA}^n$ in Lai et al.[13]), while $CMR_g$ we measured with PET was only $+52\%$ higher. Rather than a brain region-specificity, this discrepancy might thus be due to using the measured plasma lactate levels in the modeling here, instead of assuming a physiological resting-state condition, i.e. assuming that all the lactate oxidized in the brain comes from brain glucose metabolism ($CMR_g \approx CMR_g(ox)$).

Another striking difference resides in the relatively higher level of GABA synthesis observed ($V_{GAD} = 0.32 \pm 0.06\,\mu mol/g/min$) as compared to Lizarbe et al.[28] ($V_{GABA} = 0.13 \pm 0.01\,\mu mol/g/min$), where a 1-comparment model of GABA metabolism was used after infusion of $[1,6^{-13}C_2]Glc$. As mentioned above, even though we cannot exclude that this difference might arise from regional or protocol differences, GABA synthesis from GAD remains clearly proportional to the total TCA cycle ($V_{GAD}/V_{TCA} = 0.19$), in good agreement with Lizarbe et al.[28] ($V_{GABA}/V_{TCA} = 0.16$), and Duarte and Gruetter[26] ($V_{GAD}/V_{TCA} = 0.12$). These results, together with the low inhibitory neurotransmission observed relative to GAD activity in this study, strengthen the idea that GABA is primarily synthesized from glutamate arising from the TCA in GABAergic neurons, rather than recycled from glial glutamine.[45]

The present results are largely in good agreement with previous compartmentalized studies including a GABAergic compartment (Table 2) but reveal some differences. For example, the transmitochondrial flux of excitatory neurons was rather small compared to several studies[46,47] but similar to in vivo mouse data reported recently.[13] This flux was found to be zero in the GABAergic neurons, in good agreement with Duarte and Gruetter.[26] While the latter reported a neurotransmission rate of $0.16\,\mu mol/g/min$ for excitatory neurons ($V_{NT}^e$) and $0.044\,\mu mol/g/min$ for inhibitory neurons ($V_{NT}^i$), we found much smaller values ($V_{NT}^e$

of $= 0.01\,\mu mol/g/min$, $V_{NT}^i$ of $0.0007\,\mu mol/g/min$). One possible explanation may be the use of isoflurane compared to alpha-chloralose used in this study. Isoflurane has been reported to induce hyperpolarization of hippocampal pyramidal (excitatory) cells.[48] While it seems clear that the low excitatory neuron neurotransmission rate has been caused by the deep anesthesia, as has been evidenced in other studies,[15] it is less obvious how inhibitory neurotransmission is affected. It is important to note that, unlike glutamatergic neurons, neurotransmitter release in GABAergic neurons is thought to rely less on astrocytic recycling through the Glu/GABA-Gln cycle[49,50] making the net inhibitory neurotransmission more difficult to assess. This would have significant influence in the interpretation of our data: while $V_{NT}^e$ is certainly proportional to excitatory electrical activity, $V_{NT}^i$ might only reflect part of GABAergic neurotransmitter release. For instance, $V_{ex}^i$ flux, which was considered in this study for the first time, may reflect the proportion of extra-synaptic GABA reuptake by GABAergic neurons that re-enters neurotransmission pool without being further metabolized. As a result, inhibitory neurotransmission is likely to be closer to $V_{NT}^i + V_{ex}^i$ than solely $V_{NT}^i$. Following this reasoning, GABA neurotransmission would account for $\sim 13\%$ of total neurotransmission, which is in good agreement with values of $\sim 11\%$ found using $N_2/O_2$[24] or $\sim 21\%$ found with alpha-chloralose[26] in rats. Finally, GABAergic contribution to neuronal total TCA cycle was higher ($\sim 27\%$) than previously reported by Duarte and Gruetter[26] ($\sim 17\%$), van Eijsden et al.[24] ($\sim 12\%$), and Hyder et al. ($\sim 18\%$).[51] GABAergic oxidative metabolism is tightly linked to GAD activity, which contributes to GABAergic TCA ($V_{TCA}^i = V_{PDH}^i + V_{GAD} - V_{NT}^i$). Mason et al.[52] reported that $V_{GAD}$ is related to the level of GAD67 protein and was measured to be $0.10–0.15\,\mu mol/g/min$ in rat cortex, where GAD67 represents only $\sim 28\%$ of total GAD. The fact that GAD67 represents 50% of total GAD in mouse hippocampus[44] could explain the higher GABAergic oxidative metabolism observed here. Overall, we observed a higher glucose oxidation of inhibitory neurons ($V_{TCA}/V_{NT}$) compared to excitatory neurons (i.e. 2.30-fold), which might reflect a specificity of hippocampal GABAergic properties. A higher TCA oxidative requirement for GABAergic neurotransmission, relative to that of glutamatergic neurotransmission (1.09-fold), has been reported previously in a hippocampal area[24] as compared to cortex (0.72-fold)[15] or whole brain (0.73-fold)[26] in rats. High energy demands of hippocampal inhibitory network may provide mechanistic links to explain vulnerability of this structure to stress and psychiatric conditions.[53,54]

Another major difference is the high variability of the dilution $V_{dil}{}^g$ parameter compared to Duarte and Gruetter[26] using a three-compartment model and when applying a one-compartment model here. This flux takes into account the events that would lead to the dilution of TCA cycle-related metabolites (Glu, Gln, Asp and GABA) through the action of glial-specific metabolism that does fuel oxidation in the mitochondria, such as glycogen metabolism,[10] or that involves labeling contribution from blood acetate. As the three-compartment model includes other possible diluting mechanisms, i.e. through dilution from the GABA exchange flux ($V_{ex}{}^i$) as well as the glutamine exchange flux ($V_{ex}{}^g$), $V_{dil}{}^g$ drops when the model considers the existence of only one-Gln or one-GABA pool. Because previously reported dilution fluxes[11,13] (0.5-1 μmol/g/min) do not seem realistic in terms of glial metabolism (i.e. glycogen breakdown, acetate uptake, etc.), our results strongly suggest that dilution occurs at another level than arising from glial AcCoA.

## Incorporation of FEs of blood glucose, lactate and acetate for an accurate assessment of brain energetic fluxes

In this study, a higher $CMR_g(ox)$ (= $V_{TCA}/2$) relative to $CMR_g$ was observed when compared to other studies.[13,26] This difference might partially arise from the incorporation of lactate dynamics in the model here.[55] Instead of setting the net brain lactate influx from blood ($V_{dil}{}^{in} - V_{dil}{}^{out}$) to be dependent on the estimated $CMR_g(ox)$ and the fixed $CMR_g$, we measured and considered the FE and concentration of blood Lac. Generally, a net efflux of lactate is observed upon glucose consumption from the brain, in other words $CMR_g > CMR_g(ox)$.[56] However, at the end of the experiment, the high levels of peripheral Lac (∼8mM) and brain Lac (∼2.7mM) resulted in a $Lac_{brain}/Lac_{blood}$ ratio of ∼0.3 and altered the directionality of lactate flux to be from the blood to the brain. Since this effect is amplified by the permeabilization properties of isoflurane on the blood–brain barrier,[57] the determination of the FE and concentration of blood Lac in the model improves the assessment of brain energetic fluxes. While blood glucose labeling was comparable to that of brain glucose with a rapid rise after 20 min, lactate and acetate reached a FE of 0.50 only after ∼150 min of infusion. As a result, including these dynamic labeling curves of blood metabolites, rather than a fixed FE value, in the flux analysis led to an improved fitting quality and modeling reliability.

## General concerns in anesthesia and modeling

Isoflurane is a gold-standard versatile anesthesia for mice; however, it may affect brain activity stronger than other anesthetics and cause substantial changes in metabolic fluxes.[48] For instance, a relatively low $V_{NT}$ was measured with both models, which may be partially explained by reduced electrical activity induced by the effects of such anesthesia.[58] While isoflurane remains the most commonly used volatile anesthetic agent in rodents and presents clear technical advantages by its ease of use, encouraging the use of other anesthetics for ^{13}C-MRS experiments in mouse will further widen our understanding in the effect of these chemicals on metabolic fluxes. It should be noted that although anesthesia levels were comparable between [18]FDG-PET and ^{1}H-[^{13}C]-MRS studies, glycemic differences might limit the interpretation of the results. In particular, due to low sensitivity of ^{13}C nucleus, glucose infusion during ^{1}H-[^{13}C]-MRS experiments is normally performed using a hyperglycemic clamp (i.e. by inducing a steady-state hyperglycemia for a given period).[30] Although this hyperglycemic protocol is based on the idea that glucose brain entry and metabolism are not dependent on blood glucose when its concentration is above a certain threshhold,[59] it might have unwanted physiological effects on the brain metabolism, like a reduction of $CMR_g$ or alteration of plasma insulin levels,[59,60] and the impact of the extended period of hyperglycemia on glucose metabolic rates cannot be excluded[60] and remain to be further explored. On the contrary, [18]FDG-PET experiment is performed in a euglycemic condition without prior fasting that is reflecting normal physiological status of metabolism and function. Nevertheless, our approach aims at preventing non-physiological consequences of hyperglycemia on the ^{1}H-[^{13}C]-MRS metabolic flux estimation by setting the $CMR_g$ in the mathematical model to a physiological value, i.e. obtained from the PET experiment. Thus, combining [18]FDG-PET with ^{1}H-[^{13}C]-MRS provides a useful approach to determine brain metabolic fluxes in vivo.

Another point to be mentioned is that increasing the complexity of the mathematical model allows a better fitting of the data but may lead to several flux estimations to be close to zero. Even though the addition of these parameters might appear impractical, the proposed model with increased complexity remains very helpful to seek specific metabolic differences in comparative animal studies. Nevertheless, it is primordial that the prior knowledge of the model is motivated by biological evidences and a priori knowledge that support the approximations and assumptions made in the mathematical modeling. Inclusion of additional blood labeling information significantly improved the

modeling outcomes, and thus, working towards a real-time quantification of plasma metabolite concentration and labeling, i.e. during the MRS acquisition, may further strengthen the modeling precision.

## Conclusion

We conclude that quantification of $^1$H-[$^{13}$C]-labeled metabolites at 14 T during [U-$^{13}$C$_6$]Glc infusion can be improved. With a joint $^{18}$FDG-PET measurement and additional blood labeling analysis, a metabolic flux analysis distinguishing GABAergic and glutamatergic neuronal metabolism was possible using a three-compartment model with fixed glial parameters. We report that under our experimental conditions, glucose oxidation relative to neurotransmission was more important for inhibitory neurons than excitatory neurons. This result might have significant implications for the understanding of metabolic resilience of the hippocampal GABAergic system. Taken together, our results provide new tools typically applicable in comparative studies of mouse brain with glutamatergic/GABAergic metabolic imbalance.

### Declaration of conflicting interests

The author(s) declare no potential conflicts of interest with respect to the research, authorship, and/or publication of this article.

### Authors' contributions

AC, HL, BLi and RG designed the study. AC, CPY and BLa acquired and analyzed the data. AC, HL, BLi, CPY, BLa, GD and RG interpreted the data. AC drafted the manuscript. HL, BLi, CPY, BLa, GD and RG assisted in revising the manuscript and approved the final version.

### ORCID iDs

Antoine Cherix https://orcid.org/0000-0002-4168-8273
Blanca Lizarbe https://orcid.org/0000-0002-5531-4088
Hongxia Lei https://orcid.org/0000-0002-4065-9331

### Supplemental material

Supplemental material for this article is available online.

## References

1. Picard M, McManus MJ, Gray JD, et al. Mitochondrial functions modulate neuroendocrine, metabolic, inflammatory, and transcriptional responses to acute psychological stress. *Proc Natl Acad Sci U S A* 2015; 112: E6614–E6623.

2. Osborne DM, Pearson-Leary J and McNay EC. The neuroenergetics of stress hormones in the hippocampus and implications for memory. *Front Neurosci* 2015; 9: 1–16.

3. Veeraiah P, Noronha JM, Maitra S, et al. Dysfunctional glutamatergic and γ-aminobutyric acidergic activities in prefrontal cortex of mice in social defeat model of depression. *Biol Psychiatry* 2014; 76: 231–238.

4. Krystal JH, Sanacora G, Blumberg H, et al. Glutamate and GABA systems as targets for novel antidepressant and mood-stabilizing treatments. *Mol Psychiatry* 2002; 7: S71–S80.

5. Larrieu T, Cherix A, Duque A, et al. Hierarchical status predicts behavioral vulnerability and nucleus accumbens metabolic profile following chronic social defeat stress. *Curr Biol* 2017; 27: 2202–2210.e4.

6. Kim S-Y, Lee Y-J, Kim H, et al. Desipramine attenuates forced swim test-induced behavioral and neurochemical alterations in mice: an in vivo(1)H-MRS study at 9.4T. *Brain Res* 2010; 1348: 105–113.

7. Shulman RG, Brown TR, Ugurbil K, et al. Cellular applications of 31P and 13C nuclear magnetic resonance. *Science* 1979; 205: 160–166.

8. Neurohr KJ, Barrett EJ, Shulman RG. In vivo carbon-13 nuclear magnetic resonance studies of heart metabolism. *Proc Natl Acad Sci U S A* 1983; 80: 1603–1607.

9. Mason GF, Behar KL, Rothman DL, et al. NMR determination of intracerebral glucose concentration and transport kinetics in rat brain. *J Cereb Blood Flow Metab* 1992; 12: 448–455.

10. Duarte JMN, Lanz B and Gruetter R. Compartmentalized cerebral metabolism of [1,6- 13C]glucose determined by in vivo 13C NMR spectroscopy at 14.1 T. *Front Neuroenergetics* 2011; 3: 1–15.

11. Lanz B, Gruetter R and Duarte JMN. Metabolic flux and compartmentation analysis in the brain in vivo. *Front Endocrinol* 2013; 4: 1–18.

12. Sonnay S, Poirot J, Just N, et al. Astrocytic and neuronal oxidative metabolism are coupled to the rate of glutamate-glutamine cycle in the tree shrew visual cortex. *Glia* 2018; 66: 477–491.

13. Lai M, Lanz B, Poitry-Yamate C, et al. In vivo 13C MRS in the mouse brain at 14.1 Tesla and metabolic flux quantification under infusion of [1,6-13C2]glucose. *J Cereb Blood Flow Metab* 2018; 38: 1701–1714.

14. Lanz B, Xin L, Millet P, et al. In vivo quantification of neuro-glial metabolism and glial glutamate concentration using 1H-[13C] MRS at 14.1T. *J Neurochem* 2014; 128: 125–139.

15. Patel AB, de Graaf RA, Mason GF, et al. The contribution of GABA to glutamate/glutamine cycling and energy metabolism in the rat cortex in vivo. *Proc Natl Acad Sci U S A* 2005; 102: 5588–5593.

16. Pfeuffer J, Tkác I, Choi IY, et al. Localized in vivo 1H NMR detection of neurotransmitter labeling in rat brain during infusion of [1-13C] D-glucose. *Magn Reson Med* 1999; 41: 1077–1083.

17. de Graaf RA, Brown PB, Mason GF, et al. Detection of [1,6-13C2]-glucose metabolism in rat brain by in vivo1H-[13C]-NMR spectroscopy. *Magn Reson Med* 2003; 49: 37–46.

18. Deelchand DK, Nelson C, Shestov AA, et al. Simultaneous measurement of neuronal and glial metabolism in rat brain in vivo using co-infusion of [1,6-13C2] glucose and [1,2-13C2]acetate. *J Magn Reson* 2009; 196: 157–63.

19. Manor D, Rothman DL, Mason GF, et al. The rate of turnover of cortical GABA from [1-13C]glucose is reduced in rats treated with the GABA-transaminase inhibitor vigabatrin (γ-vinyl GABA). *Neurochem Res* 1996; 21: 1031–1041.

20. de Graaf RA, Patel AB, Rothman DL, et al. Acute regulation of steady-state GABA levels following GABA-transaminase inhibition in rat cerebral cortex. *Neurochem Int* 2006; 48: 508–514.

21. Tiwari V, Ambadipudi S and Patel AB. Glutamatergic and GABAergic TCA cycle and neurotransmitter cycling fluxes in different regions of mouse brain. *J Cereb Blood Flow Metab* 2013; 33: 1523–1531.

22. Gruetter R, Novotny EJ, Boulware SD, et al. Localized 13C NMR spectroscopy in the human brain of amino acid labeling from D-[1-13C]glucose. *J Neurochem* 1994; 63: 1377–85.

23. Beckmann N, Turkalj I, Seelig J, et al. Carbon-13 NMR for the assessment of human brain glucose metabolism in vivo. *Biochemistry* 1991; 30: 6362–6366.

24. van Eijsden P, Behar KL, Mason GF, et al. In vivo neurochemical profiling of rat brain by 1H-[13C] NMR spectroscopy: cerebral energetics and glutamatergic/GABAergic neurotransmission. *J Neurochem* 2010; 112: 24–33.

25. Yang J, Li CQ and Shen J. In vivo detection of cortical GABA turnover from intravenously infused [1-13C]D-glucose. *Magn Reson Med* 2005; 53: 1258–1267.

26. Duarte JMN and Gruetter R. Glutamatergic and GABAergic energy metabolism measured in the rat brain by 13 C NMR spectroscopy at 14.1 T. *J Neurochem* 2013; 126: 579–590.

27. Xin L, Lanz B, Lei H, et al. Assessment of metabolic fluxes in the mouse brain in vivo using 1 H-[13 C] NMR spectroscopy at 14.1 Tesla. *J Cereb Blood Flow Metab* 2015; 35: 759–765.

28. Lizarbe B, Lei H, Duarte JMN, et al. Feasibility of in vivo measurement of glucose metabolism in the mouse hypothalamus by 1H-[13C] MRS at 14.1T. *Magn Reson Med* 2018; 80: 874–884.

29. Lizarbe B, Cherix A, Duarte JMN, et al. High-fat diet consumption alters energy metabolism in the mouse hypothalamus. *Int J Obes* 2019; 43: 1295–1304.

30. Henry PG, Adriany G, Deelchand D, et al. In vivo 13C NMR spectroscopy and metabolic modeling in the brain: a practical perspective. *Magn Reson Imaging* 2006; 24: 527–539.

31. Adriany G and Gruetter R. A half-volume coil for efficient proton decoupling in humans at 4 tesla. *J Magn Reson* 1997; 125: 178–84.

32. Gruetter R and Tkáč I. Field mapping without reference scan using asymmetric echo-planar techniques. *Magn Reson Med* 2000; 43: 319–323.

33. Xin L, Lanz B, Frenkel H, et al. BISEP-based, Ultra-short TE 1 H– [13 C] NMR Spectroscopy of the Rat Brain at 14.1 T, www.jstage.jst.go.jp/browse/islsm (2009, accessed 21 February 2020).

34. Tannüs A and Garwood M. Improved performance of frequency-swept pulses using offset-independent adiabaticity. *J Magn Reson* 1996; 120: 133–137.

35. Fujiwara T, Anai T, Kurihara N, et al. Frequency-switched composite pulses for decoupling carbon-13 spins over ultrabroad bandwidths. *J Magn Reson Ser A* 1993; 104: 103–105.

36. Provencher SW. Automatic quantitation of localized in vivo 1H spectra with LCModel. *NMR Biomed* 2001; 14: 260–264.

37. Kunz N, Cudalbu C, Mlynarik V, et al. Diffusion-weighted spectroscopy: a novel approach to determine macromolecule resonances in short-echo time 1H-MRS. *Magn Reson Med* 2010; 64: 939–946.

38. Mlynárik V, Cudalbu C, Xin L, et al. 1H NMR spectroscopy of rat brain in vivo at 14.1 Tesla: improvements in quantification of the neurochemical profile. *J Magn Reson* 2008; 194: 163–168.

39. Cavassila S, Deval S, Huegen C, et al. Cramér-Rao bounds: an evaluation tool for quantitation. *NMR Biomed* 2001; 14: 278–283.

40. Folch J, Lees M and Sloane Stanley GH. A simple method for the isolation and purification of total lipides from animal tissues. *J Biol Chem* 1957; 226: 497–509.

41. Lanz B, Poitry-Yamate C and Gruetter R. Image-derived input function from the vena cava for 18F-FDG PET studies in rats and mice. *J Nucl Med* 2014; 55: 1380–1388.

42. Waagepetersen HS, Sonnewald U, Larsson OM, et al. Multiple compartments with different metabolic characteristics are involved in biosynthesis of intracellular and released glutamine and citrate in astrocytes. *Glia* 2001; 35: 246–52.

43. Martin DL and Rimvall K. Regulation of gamma-aminobutyric acid synthesis in the brain. *J Neurochem* 1993; 60: 395–407.

44. Sheikh S, Martin S and Martin D. Regional distribution and relative amounts of glutamate decarboxylase isoforms in rat and mouse brain. *Neurochem Int* 1999; 35: 73–80.

45. Schousboe A and Waagepetersen HS. GABA: homeostatic and pharmacological aspects. *Prog Brain Res* 2007; 160: 9–19.

46. Sibson NR, Dhankhar A, Mason GF, et al. Stoichiometric coupling of brain glucose metabolism and glutamatergic neuronal activity. *Proc Natl Acad Sci U S A* 1998; 95: 316–321.

47. Mason GF, Gruetter R, Rothman DL, et al. Simultaneous determination of the rates of the TCA cycle, glucose utilization, alpha-ketoglutarate/glutamate

exchange, and glutamine synthesis in human brain by NMR. *J Cereb Blood Flow Metab* 1995; 15: 12–25.

48. Berg-Johnsen J and Langmoen IA. Mechanisms concerned in the direct effect of isoflurane on rat hippocampal and human neocortical neurons. *Brain Res* 1990; 507: 28–34.

49. Schousboe A, Bak LK and Waagepetersen HS. Astrocytic control of biosynthesis and turnover of the neurotransmitters glutamate and GABA. *Front Endocrinol* 2013; 4: 102.

50. Sonnewald U, Westergaard N, Schousboe A, et al. Direct demonstration by [13C]NMR spectroscopy that glutamine from astrocytes is a precursor for GABA synthesis in neurons. *Neurochem Int* 1993; 22: 19–29.

51. Hyder F, Patel AB, Gjedde A, et al. Neuronal-glial glucose oxidation and glutamatergic-GABAergic function. *J Cereb Blood Flow Metab* 2006; 26: 865–877.

52. Mason GF, Martin DL, Martin SB, et al. Decrease in GABA synthesis rate in rat cortex following GABA-transaminase inhibition correlates with the decrease in GAD67 protein. *Brain Res* 2001; 914: 81–91.

53. Steiner J, Brisch R, Schiltz K, et al. GABAergic system impairment in the hippocampus and superior temporal gyrus of patients with paranoid schizophrenia: a post-mortem study. *Schizophr Res* 2016; 177: 10–17.

54. Hu W, Zhang M, Czéh B, et al. Stress impairs GABAergic network function in the hippocampus by activating non-genomic glucocorticoid receptors and affecting the integrity of the parvalbumin-expressing neuronal network. *Neuropsychopharmacology* 2010; 35: 1693–1707.

55. Boumezbeur F, Petersen KF, Cline GW, et al. The contribution of blood lactate to brain energy metabolism in humans measured by dynamic 13C nuclear magnetic resonance spectroscopy. *J Neurosci* 2010; 30: 13983–13991.

56. Patel AB, de Graaf RA, Mason GF, et al. Glutamatergic neurotransmission and neuronal glucose oxidation are coupled during intense neuronal activation. *J Cereb Blood Flow Metab* 2004; 24: 972–985.

57. Acharya NK, Goldwaser EL, Forsberg MM, et al. Sevoflurane and Isoflurane induce structural changes in brain vascular endothelial cells and increase blood−brain barrier permeability: possible link to post-operative delirium and cognitive decline. *Brain Res* 2015; 1620: 29–41.

58. Choi IY, Lei H and Gruetter R. Effect of deep pentobarbital anesthesia on neurotransmitter metabolism in vivo: on the correlation of total glucose consumption with glutamatergic action. *J Cereb Blood Flow Metab* 2002; 22: 1343–1351.

59. Duckrow RB and Bryan RM. Regional cerebral glucose utilization during hyperglycemia. *J Neurochem* 1987; 48: 989–993.

60. DeFronzo RA, Tobin JD and Andres R. Glucose clamp technique: a method for quantifying insulin secretion and resistance. *Am J Physiol Metab* 1979; 237: E214.